Anomalous Segment Diffusion in Polymers and NMR Relaxation Spectroscopy

Hans Werner Weber and Rainer Kimmich*

Sektion Kernresonanzspektroskopie, Universität Ulm, 89069 Ulm, Germany

Received July 15, 1992; Revised Manuscript Received January 11, 1993

ABSTRACT: The dynamics of polymer chains in melts, solutions, and networks was studied by the aid of NMR relaxation spectroscopy. Proton data of the spin–lattice relaxation times in the laboratory and rotating frames, T_1 and $T_{1\rho}$, respectively, and of transverse relaxation curves are reported. Frequency, temperature, concentration, molecular weight, and cross-link density dependences have been investigated. T_1 was measured in a frequency range of 10^3 to 3×10^8 Hz predominantly using the field-cycling technique. The study refers to polyisoprene, polyisobutylene, poly(tetrahydrofuran), polystyrene, poly(ethylene oxide), polyethylene, and poly(dimethylsiloxane). The range of molecular weights was 10^3–10^6. The power laws for the time dependence of the mean-square displacement, $\langle r^2 \rangle \propto t^{1/2}$ and $\langle r^2 \rangle \propto t^{1/4}$, predicted by the Doi/Edwards tube model for coil–internal segment diffusion are shown to have their counterparts in the frequency dependence of the spin–lattice relaxation time which is characterized by power laws $T_1 \propto \omega^{0.5}$ and $T_1 \propto \omega^{0.25}$ in corresponding dynamic ranges. The experimental data can be interpreted on the basis of three components of segment fluctuations. The crucial process is the reorientation of segments as a consequence of translational displacements. The orientation correlation function for this mechanism can be derived directly from limits of the time dependence of the mean-square segment displacements provided that the displacements are guided by the chain contour. The experiments show, on the other hand, that the chain dynamics in length scales less than the Doi/Edwards tube diameter is not compatible with the Rouse model, whereas that of melts below the critical molecular weight and solutions is.

Introduction

The tube model of polymer dynamics[1,2] is characterized by a number of peculiar power laws referring to translational diffusion. Among these the time, molecular weight, and concentration dependences of the mean-square displacements of segments in short length scales are of particular interest. The characteristic length scales are defined by the length of a Kuhn segment, b, the step length of the primitive path, a, and the radius of gyration, $R_g = b(N/6)^{1/2}$, where N is the number of Kuhn segments per chain.

The time scales of diffusion are specified by certain time constants corresponding to these length scales. The elementary segment reorientation time characterizing rotationally restricted segment motions is $\tau_s = \zeta b^2/(k_B T)$, where ζ is the friction coefficient of a Kuhn segment, k_B is Boltzmann's constant, and T is the absolute temperature. The time constant $\tau_e = N_e^2 \tau_s/(3\pi^2)$ represents the period during which lateral displacements occur not yet influenced by the tube constraint effect. $N_e = a^2/b^2$ is the number of Kuhn segments corresponding to the so-called entanglement length. The definition of τ_e refers to the (longest) Rouse relaxation time of a chain fragment with N_e segments. After the (longest) Rouse relaxation time of the whole chain consisting of N Kuhn segments, $\tau_R = N^2 \tau_s/(3\pi^2)$, *coherent* motions (with respect to different chain parts[3]) become relevant. The time $\tau_d = N^3 \tau_s c^{3/2}/(\pi^2 N_e)$ finally characterizes the tube disengagement process. c is the polymer concentration.

With these definitions the following limits for the mean-square displacement behavior are expected in the frame of the Doi/Edwards model.[1]

Limit I $(\tau_s \ll t \ll \tau_e$ or $b^2 \ll \langle r^2 \rangle \ll a^2)$:

$$\langle r^2 \rangle = 3^{1/2} \pi b^2 (t/\tau_s)^{1/2} \tag{1}$$

Limit II $(\tau_e \ll t \ll \tau_R$ or $a^2 \ll \langle r^2 \rangle \ll 6^{1/2} R_g a)$:

$$\langle r^2 \rangle = 3^{1/4} \pi^{1/2} b^2 N_e^{1/2} (t/\tau_s)^{1/4} \tag{2}$$

Limit III $(\tau_R \ll t \ll \tau_d$ or $6^{1/2} R_g a \ll \langle r^2 \rangle \ll 6 R_g^2)$:

$$\langle r^2 \rangle = \pi b^2 (N_e t/N \tau_s)^{1/2} \tag{3}$$

Limit IV $(t \gg \tau_d$ or $6R_g^2 \ll \langle r^2 \rangle)$:

$$\langle r^2 \rangle = 6Dt \tag{4}$$

where $D = \pi^2 a^2 k_B T/(6 b^2 \zeta N^2)$ is the center-of-mass self-diffusion coefficient of the chain.[1,2,4,5]

Using the NMR (nuclear magnetic resonance) field-gradient[6–9] and neutron spin-echo scattering[10,11] techniques, evidence for a part of the coil–internal limits of the mean-square displacement behavior has been found for semidilute solutions as well as for melts. While the time/length scale of the NMR field-gradient method is at the "long" side of the above limits, that of neutron spin-echo scattering is at the "short" side. The gap in between is favorably covered by nuclear magnetic relaxation spectroscopy, especially in the field-cycling version.[12,13]

In previous reports[14–16] it was already shown that a major relaxation mechanism is caused by reorientations mediated

0024-9297/93/2226-2597$04.00/0

by translational displacements of segments. The corresponding process contributes as "component B" to the segment orientation correlation function. Spin–lattice relaxation in the laboratory[15] and rotating[16–18] frames and transverse relaxation recorded without[15] or with[19] multipulse narrowing in polymer melts have been evaluated on this basis.

The present NMR relaxation study extends the investigations to a wide variety of different polymers. The data refer to molten linear polyisoprene (PIP), polyisobutylene (PIB), poly(ethylene oxide) (PEO), polyethylene (PE), polystyrene (PS), poly(tetrahydrofuran) (PTHF), and linear as well as cross-linked poly(dimethylsiloxane) (PDMS) recorded with samples in a broad range of molecular weights and mesh sizes. The objective is to explain the dependences on the frequency, the molecular weight, the temperature, and the concentration with a concept of chain dynamics as close as possible.

Under the usual assumptions the spin–lattice relaxation rates $1/T_1$ and $1/T_{1\rho}$ in the laboratory and rotating frames of references, respectively, are given by[20,21]

$$\frac{1}{T_1} \approx \left(\frac{\mu_0}{4\pi}\right)^2 \frac{3}{2}\gamma^4\hbar^2 I(I+1)\langle|F^{(1)}|^2\rangle[\mathcal{J}(\omega_0) + 4\mathcal{J}(2\omega_0)] \quad (5)$$

$$\frac{1}{T_{1\rho}} \approx \left(\frac{\mu_0}{4\pi}\right)^2 \frac{3}{4}\gamma^4\hbar^2 I(I+1)\langle|F^{(1)}|^2\rangle[3\mathcal{J}(2\omega_1) + 5\mathcal{J}(\omega_0) + 2\mathcal{J}(2\omega_0)] \quad (6)$$

where we have anticipated dipolar interaction. That is, $F^{(1)} = r^{-3} \sin\theta \cos\theta \exp(i\phi)$. r, θ, and ϕ are spherical coordinates characterizing internuclear vectors of nearest neighbors. γ is the gyromagnetic ratio, $\hbar$ is Planck's constant divided by 2π, and μ_0 is the magnetic field constant. $\omega_0 = 2\pi\nu_0 = \gamma B_0$ and $\omega_1 = 2\pi\nu_1 = \gamma B_1$ are the circular Larmor frequencies in the external field B_0 and the rotating radio-frequency field B_1, respectively. (The indices of the frequencies will be omitted in the following.) The intensity function $\mathcal{J}(\omega)$ is the Fourier transform of the reduced correlation function $G(t)$. At least at long times (or low frequencies) intermolecular interaction is negligible so that $G(t)$ can essentially be identified with the orientation correlation function of the interacting spin pairs within the chain segments.

With polymers, transverse relaxation normally occurs under conditions of incomplete motional narrowing. The decay of the transverse magnetization signal, $S(t)$, can then be described by the Anderson/Weiss/Kubo/Tomita formula[20]

$$S(t) = S(0) \exp\{-M_2\int_0^t (t-\tau)G_\omega(\tau)\,d\tau\} \quad (7)$$

M_2 is the second moment of the line expected in the absence of the molecular motions. As a reasonable approximation, the reduced correlation function of the local Larmor frequency, $G_\omega(\tau)$, can be identified with the orientation correlation function, $G(t)$, of spin–lattice relaxation.

Taking all three methods together, transverse relaxation and spin–lattice relaxation in the laboratory and rotating frames, permits one to cover an extremely broad range of fluctuation rates ranging from much less than 10^2 s^{-1} to much more than 10^8 s^{-1}. An important fact is that the different measuring quantities reflect the features of essentially the same orientation correlation function so that the data can be interpreted with a common formalism.

Instruments and Samples

Most of the spin–lattice relaxation experiments were carried out with the field-cycling technique.[12,13] A home-built apparatus using a liquid-nitrogen-cooled copper magnet was used. The proton frequency range was 2×10^3–2×10^7 Hz. Spin–lattice relaxation times at higher frequencies or spin–lattice relaxation times in the rotating frame were recorded with Bruker SXP 4-100 and MSL 300 spectrometers operating at 90 and 300 MHz, respectively. The control of the sample temperature was better than ±1 K. All laboratory-frame spin–lattice relaxation curves were found to be monoexponential over at least 1 or 2 decades.

Linear PDMS samples in a range of weight-averaged molecular weights M_w = 340–423 000 were purchased from Polysciences, Warrington, PA, ABCR GmbH + Co. KG, Karlsruhe, Germany, and Polymer Standard Service, Mainz, Germany. The ratio of weight-average and number-average molecular weights, M_w/M_n, of the samples originating from the latter source was specified better than 1.2.

The PDMS networks with mesh molecular weights between M_n = 700 and 20 000 used in this study are described elsewhere.[16] The polydispersity of the mesh molecular weights were in the range M_w/M_n = 1.6–1.8.

PIP (M_w = 280 000–790 000; $M_w/M_n \leq 1.12$; 95% 1,4 isomers) and PIB (M_w = 36 900–1 110 000; $M_w/M_n \leq 1.28$) were purchased from Polymer Standard Service, Mainz, Germany. PEO of $M_w = 5 \times 10^6$ and M_w = 150 000, M_w/M_n = 1.04, were obtained from Aldrich and Latek, Eppelheim, Germany, respectively. The latter company also delivered the PTHF samples in the range M_w = 22 100–500 000 ($M_w/M_n \leq 1.25$). The (atactic) PS sample (M_w = 1 150 000; M_w/M_n = 1.1) was delivered by BASF, Ludwigshafen, Germany, by courtesy.

Experimental Results

Figure 1 shows the frequency dependences of the proton spin–lattice relaxation time in the laboratory and rotating frame, T_1 and $T_{1\rho}$, respectively, measured in PDMS melts, solutions, and networks. Parameters are the molecular weight and the temperature with linear polymers and the mesh molecular weight with networks.

Figure 2a shows the temperature dependence of T_1 measured in PDMS (M_w = 250 000) at 20 and 90 MHz. No minimum is visible in the investigated temperature range.[22,23] The dynamic range where T_1 minima of polymer melts occur is governed by reorientations within the Kuhn segments (called "component A" of the fluctuations) so that the condition $\omega\tau_s \approx 1$ is fulfilled. (A further minimum may occur due to methyl group rotation.[15,24]) The absence of any minimum in the temperature range of interest indicates that motions *slower* than component A are relevant. This is in contrast to the PIP data shown in Figure 2b where a pronounced T_1 minimum is visible.

The T_1 dispersion data in Figure 1 reveal regimes governed by different power laws of the frequency. Depending on the molecular weight, the concentration, and the temperature, power laws of the form $T_1, T_{1\rho} \propto \nu^0$, $\nu^{0.25}$, and $\nu^{0.5}$ are evident. A low-frequency plateau $T_1, T_{1\rho} = const$ appears in particular for molecular weights below the critical value, $M_w \ll M_c \approx 20\,000$ (see Figure 1a).

The exponent 0.25 was observed with high molecular weights (Figure 1a), with high PDMS concentrations (Figure 1c), and with PDMS networks (Figure 1d). The proportionality $T_1 \propto \nu^{0.5}$, on the other hand, characterizes the PDMS data recorded with high molecular weights at low temperatures and/or high frequencies (Figure 1b).

At certain frequencies ν_e, a crossover from the exponent 0.25 to 0.5 at higher frequencies takes place (Figure 1b). As judged from the ν_e values, a correspondence to the entanglement time τ_e exists of the form $\tau_e = 1/(2\pi\nu_e)$. Figure 3 shows the experimental temperature dependence of τ_e determined in this way. Apart from the 213 K data point

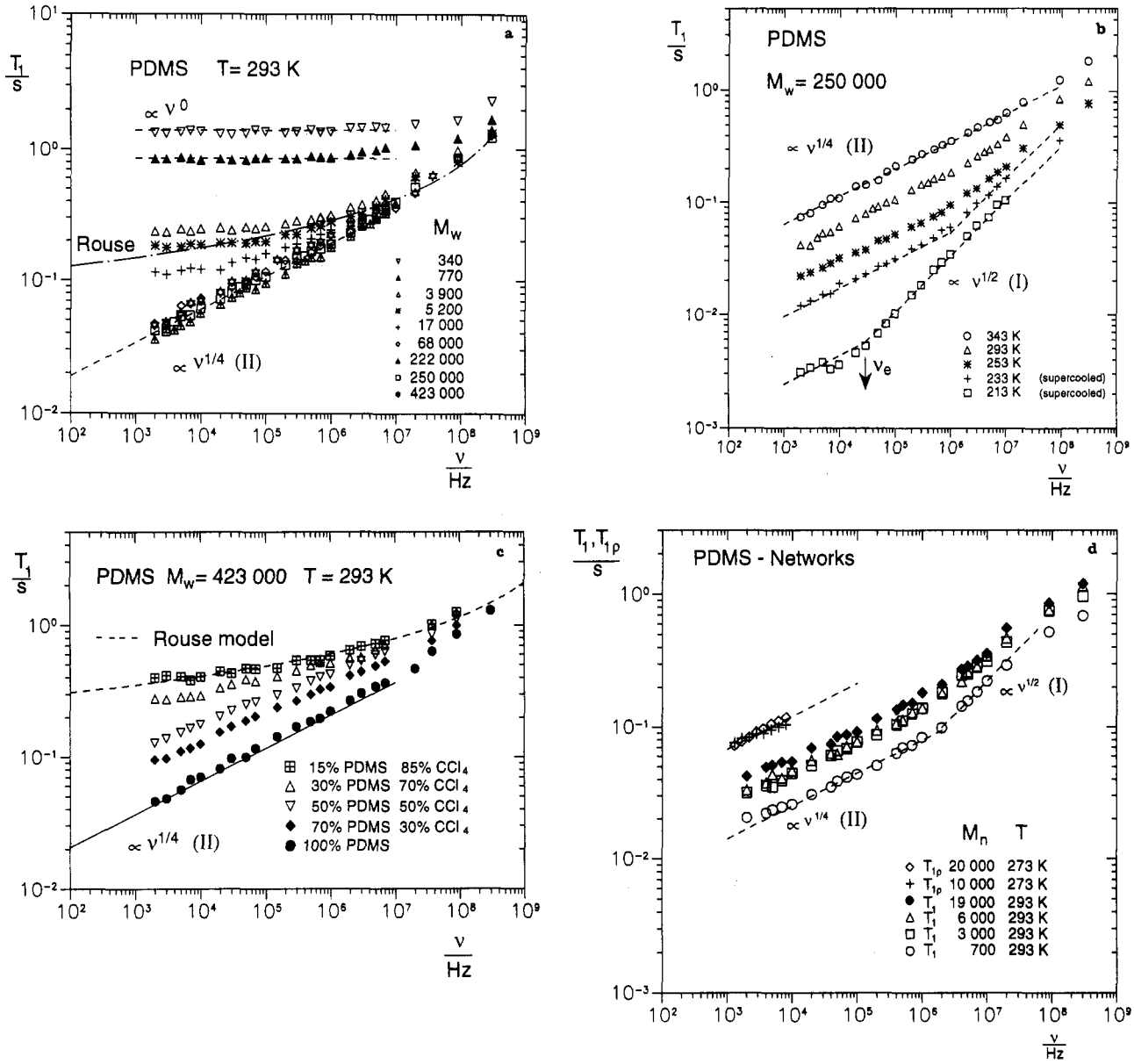

Figure 1. $T_1(\nu)$ and $T_{1\rho}(\nu)$ of PDMS melts, solutions, and networks. The indicated power laws and the Roman numbers refer to the limiting cases discussed in the text. The dispersion following from the Rouse model (eq 8) is also shown. The $T_{1\rho}$ data were recorded at a laboratory-frame Larmor frequency of 90 MHz. (a) Melts. Curve parameter: M_w (where $M_c \approx 20\,000$). The theoretical curve for the Rouse model was fitted, resulting in the parameter values $\beta = 2.1 \times 10^{-10}$ s^2 and $\tau_s = 9.8 \times 10^{-11}$ s. (b) Melts. Curve parameter: temperature. The data for temperatures below the melting point at roughly 233 K were recorded during crystallization in its seminal state. As crystallized chains are immobilized in our frequency range, the observed T_1 dispersion can be attributed to the dominating amorphous parts of the sample. Crystallization was found to be slow enough to guarantee constant measuring conditions during the experiments. (c) Solutions. Curve parameter: polymer concentration. The theoretical curve for the Rouse model was fitted, resulting in parameter values $\beta = 5.7 \times 10^{-11}$ s^2 and $\tau_s = 9.7 \times 10^{-12}$ s. (d) Networks. Curve parameter: cross-link density characterized by the molecular weight M_n of the mesh chains.

which refers to a strongly supercooled state, the data can be represented by an Arrhenius relationship. The τ_e values are close to those concluded from molecular dynamics[25] and neutron spin-echo studies.[10,11]

With PIP melts, a $\nu^{0.25}$ dispersion regime was found again (Figure 4). At low frequencies and high temperatures a crossover at a frequency ν_R from the proportionality $T_{1\rho} \propto \nu^{0.5}$ to $T_{1\rho}, T_1 \propto \nu^{0.25}$ at high frequencies is observed. Note that this third characteristic dispersion regime must be distinguished from the $\nu^{0.5}$ dispersion of the PDMS melts described above: It appears on the opposite side of the $\nu^{0.25}$ regime and—in the case of PDMS—presumably lies outside the experimental frequency window for T_1 and $T_{1\rho}$ (but not necessarily for T_2! see below). The crossover frequency corresponds to τ_R data reported in the literature[25] after correction for the different temperatures using an activation energy of 58 kJ/mol (see Figure 2). The NMR value is $\tau_R(368\text{ K}) = 1/(2\pi\nu_R) = 2 \times 10^{-5}$ s.

Above about 10^7 Hz, a tendency toward a high-frequency plateau which is attributed to local fluctuations within Kuhn segments (component A). This interpretation is supported by the temperature dependences found for T_1 (Figure 2b): For 5×10^6 Hz the T_1 minimum (which arises from just this type of local fluctuation) is close to the temperatures of the T_1 dispersion experiments, whereas it is far away from those temperatures at lower frequencies. The minimum caused by methyl group rotation is only slightly indicated at low temperatures and high frequencies far outside of the dynamic range of the T_1 and $T_{1\rho}$ dispersion experiments. This process therefore is definitely irrelevant for the T_1 dispersion study.

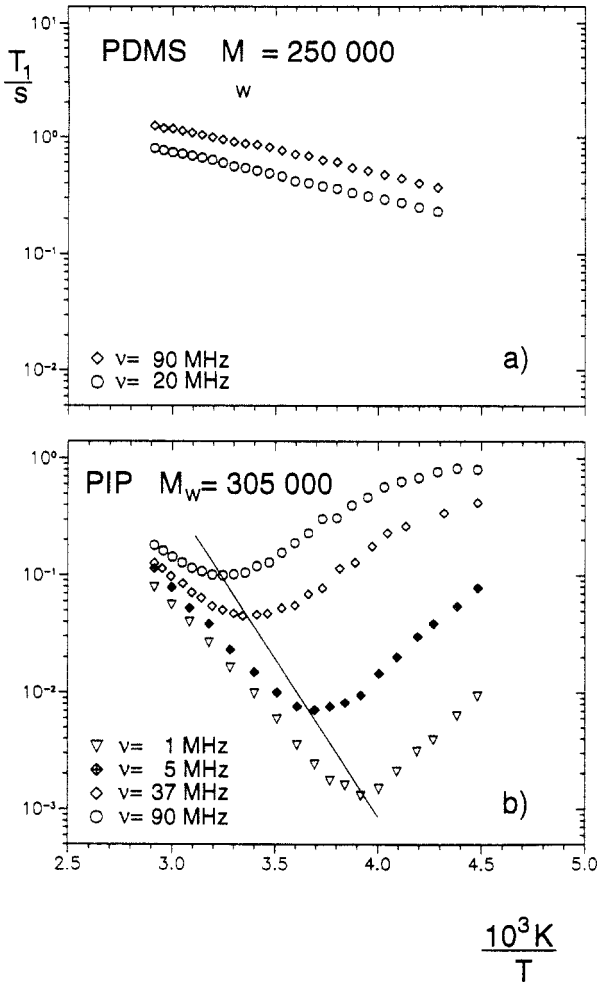

Figure 2. Temperature dependence of T_1 of (a) a PDMS and (b) a PIP melt. The curve parameter is the Larmor frequency. The condition for the minimum is $\omega\tau_s \approx 1$. T_1 dispersion data fulfilling $\omega\tau_s \ll 1$ therefore are not affected by component A. The solid line in (b) is defined by the PIP T_1 minima and corresponds to the Arrhenius law $\tau_s = \tau_{s\infty} \exp(E/RT)$ with $\tau_{s\infty} = 2 \times 10^{-19}$ s and $E = 58$ kJ/mol.

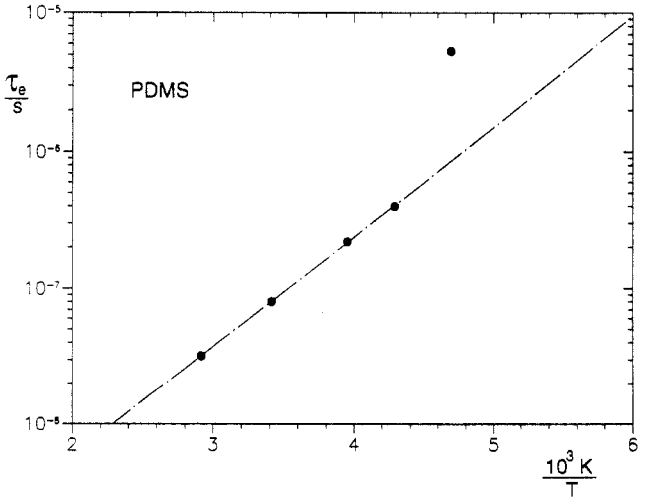

Figure 3. Arrhenius plot of τ_e evaluated from the T_1 dispersion data of PDMS (Figure 1b). The parameters of the Arrhenius law, $\tau_e = \tau_{e\infty} \exp(E/RT)$, fitted to the data are $\tau_{e\infty} = 1.1 \times 10^{-10}$ s and $E = 15.8$ kJ/mol. The deviation of the data point at 213 K indicates the influence of the supercooled state at this temperature.

PIB melts show a T_1 dispersion behavior equivalent to that of PDMS: A $\nu^{0.25}$ dependence of $T_{1\rho}$ and T_1 at low frequencies is followed by the proportionality $T_1 \propto \nu^{0.5}$

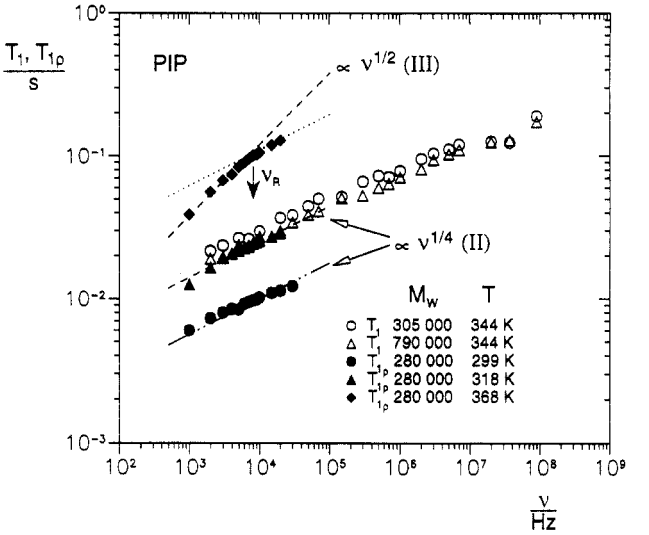

Figure 4. $T_1(\nu)$ and $T_{1\rho}(\nu)$ of PIP melts. The curve parameters are M_w ($\gg M_c$) and the temperature. The $T_{1\rho}$ data were recorded at a laboratory-frame Larmor frequency of 90 MHz. The indicated power laws and the Roman numbers refer to the limiting cases discussed in the text. At high frequencies the dispersion due to chain modes is concealed by the influence of component A (compare the T_1 minima displayed in Figure 2b).

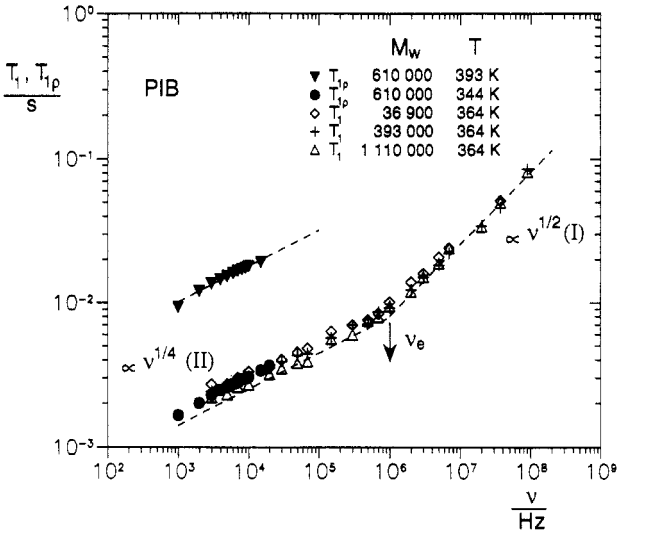

Figure 5. $T_1(\nu)$ and $T_{1\rho}(\nu)$ of PIB melts. The curve parameters are M_w ($\gg M_c$) and the temperature. The $T_{1\rho}$ data were recorded at a laboratory-frame Larmor frequency of 90 MHz. The indicated power laws and the Roman numbers refer to the limiting cases discussed in the text.

above 10^6 Hz (Figure 5). The temperature dependence[24] indicates that the T_1 and $T_{1\rho}$ dispersions are again due to processes slower than component A or methyl group rotation. From the crossover frequency one evaluates $\tau_e(364\text{ K}) = 2 \times 10^{-7}$ s.

With PTHF the situation is less clear: The data (Figure 6) indicate a $\nu^{0.25}$ dispersion in the low-frequency regime and a transition to a somewhat steeper slope at about 2×10^4 Hz which likely must be considered as the regime of a $\nu^{0.5}$ dispersion analogous to that of PDMS and PIB melts but now being strongly concealed by the superimposed influence of the local fluctuations within the Kuhn segments. The slightly sigmoidal shape of the overall dispersion seems to support this view.

The PS data (Figure 7) once more reveal a $\nu^{0.25}$ law in the low-frequency regime for $M_w \gg M_c \approx 31\,000$. At higher frequencies a tendency toward a proportionality $T_1 \propto \nu^2$ is visible which is attributed to rotational jumps of the phenyl rings. Thus the $\nu^{0.5}$ dispersion which one would

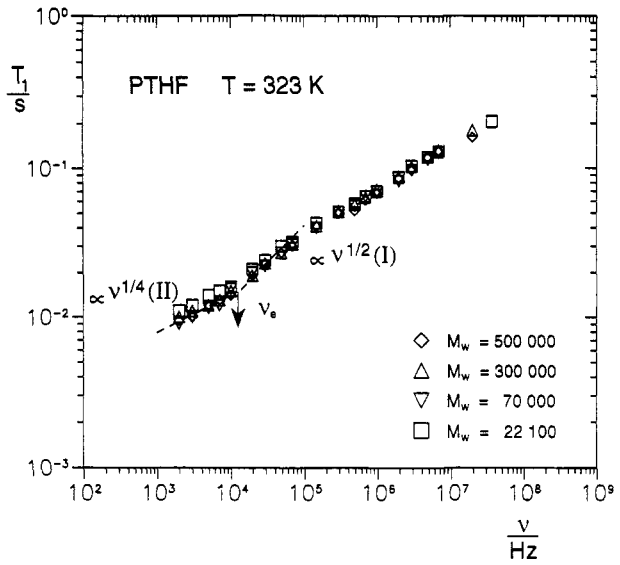

Figure 6. $T_1(\nu)$ of PTHF melts at 323 K. The curve parameter is M_w ($>M_c$). The indicated power laws refer to the limiting cases discussed in the text. The crossover to limit *I* is only slightly perceptible because of the strong influence of component A dominating at higher frequencies.

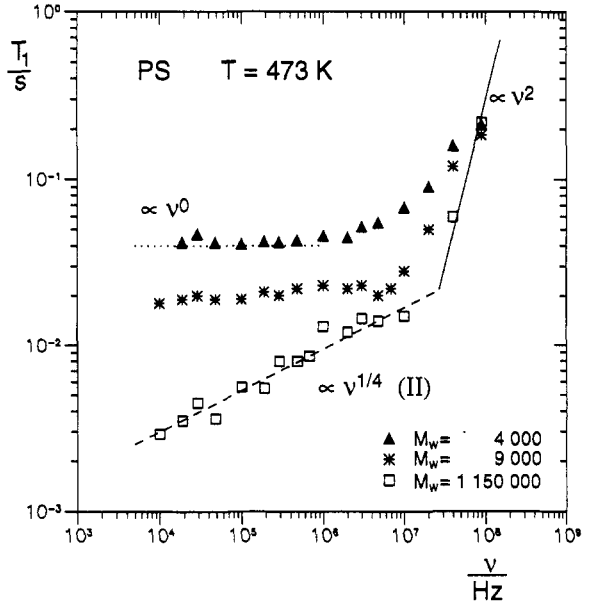

Figure 7. $T_1(\nu)$ of PS melts at 473 K. The low-frequency dispersion of the sample above $M_c \approx 31\,000$ is governed by limit II. The data above 2×10^7 Hz are influenced by local processes such as rotational jumps of phenyl groups.

expect at high frequencies in analogy to the PDMS and PIB data is concealed by this motion.

PE[15] and PEO melts (Figure 8) show a low-frequency dispersion, which can be characterized by the proportionality $T_1 \propto \nu^{0.5}$ for $M_w \gg M_c$ (4000 and 5800, respectively). Close to or below M_c a low-frequency plateau was observed.[15] Above 10^6 Hz, the slope of the T_1 dispersion flattens. This must be explained by the tendency toward a plateau due to component A. On the other hand, a $\nu^{0.25}$ dispersion region in analogy to that of PDMS and PIB obviously is beyond the low-frequency edge of the experimental frequency window of T_1 (but not necessarily of T_2!).

The exponents fitted to the low-frequency relaxation dispersion data of polymer melts with $M_w \gg M_c$ are listed in Table I. The time constants τ_s, τ_e, and τ_R can directly be evaluated from the conditions $\omega\tau_s = 1$, $\omega\tau_e = 1$, and $\omega\tau_R = 1$ indicating the T_1 minimum (due to component A), the

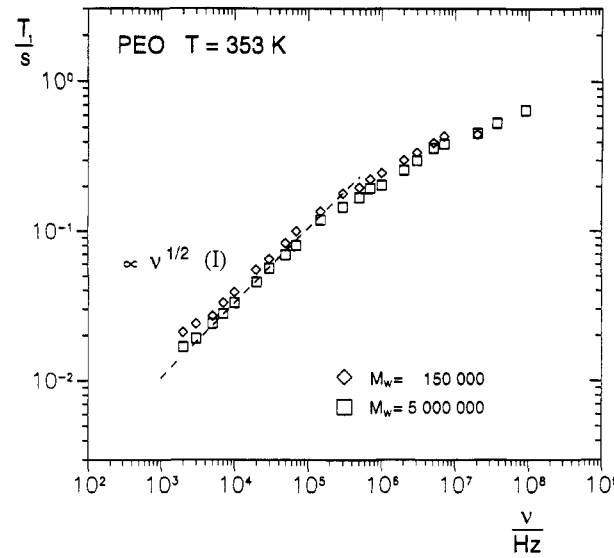

Figure 8. $T_1(\nu)$ of PEO melts at 353 K. The curve parameter is M_w ($\gg M_c \approx 5800$). At low frequencies the dispersion is governed by limit I. The flattening of the T_1 dispersion above 10^6 Hz is attributed to the influence of component A.

Table I. Exponents of the Power Laws T_1, $T_{1\rho} \propto \nu^x$ Describing the Low-Frequency Dispersion of the Experimental Spin–Lattice Relaxation Data of Polymer Melts with $M_w \gg M_c$

polymer	$x(T_{1\rho}$ data)	$x(T_1$ data)
PDMS	0.25 ± 0.05	0.24 ± 0.01
PIB	0.27 ± 0.01	0.24 ± 0.01
PS		0.26 ± 0.02
PTHF		0.25 ± 0.03
PIP (≤344 K)	0.27 ± 0.06	0.22 ● 0.01
PIP (368 K)	0.5 ● 0.05	
PE		0.52 ± 0.02
PEO		0.46 ± 0.01

Table II. Representative Values of the Characteristic Time Constants Directly Evaluated from Experimental Data (without Any Fits of Model Curves)[a]

polymer	T/K	τ_s/s	τ_e/s	τ_R/s	ref
PDMS	200	2.6×10^{-9}			26
	300		7×10^{-8}		Figure 3
PIB	263	1.6×10^{-5}			27
	345	1.8×10^{-9}			24
	364		2×10^{-7}		Figure 5
	453			5×10^{-5} (M_w = 200 000)	28
PTHF	323		9×10^{-6}		Figure 6
PIP	368	3.6×10^{-11}		2×10^{-5} (M_w = 280 000)	Figure 4

[a] τ_s: From T_1 or $T_{1\rho}$ minima ($M_w \gg M_c$) using the condition $\omega\tau_s = 1$. τ_e: From the crossover $T_1 \propto \nu^{0.25}$ (limit II) to $T_1 \propto \nu^{0.5}$ (limit I) using the condition $\omega\tau_e = 1$. τ_R: From the crossover $T_{1\rho} \propto \nu^{0.5}$ (limit III) to $T_{1\rho} \propto \nu^{0.25}$ (limit II) using the condition $\omega\tau_R = 1$.

crossover of the T_1 dispersion $\nu^{0.25} \rightarrow \nu^{0.5}$, and the crossover $\nu^{0.5} \rightarrow \nu^{0.25}$, respectively. Representative results are listed in Table II.

Transverse relaxation curves of polymers cannot generally be described by monoexponential decay curves in contrast to spin–lattice relaxation. This is partly due to incomplete motional narrowing (see eq 7). A more severe reason is however due to the dynamic three-block structure of the chains.[29] Figure 9 shows representative decays of a PDMS melt. For the convenient representation of the molecular weight and temperature dependences, the "transverse relaxation time" T_2 was defined and evaluated as the decay time to $1/e$ of the initial value. Experimental data have been reported elsewhere.[15,16,24]

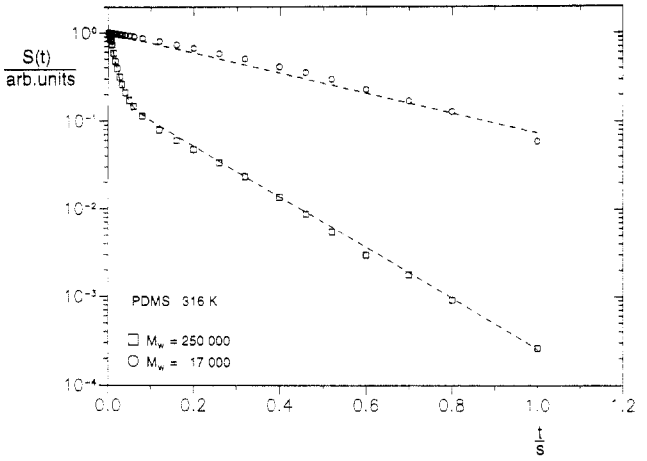

Figure 9. Transverse relaxation decays of PDMS melts measured[29] at 316 K using the Hahn spin-echo method. The broken lines have been calculated using eqs 21 and 23. Above M_c the different dynamics of chain-end (slow component) and chain-middle (fast component) blocks reveal themselves. $A(t)$ was approximated by the residual correlation a_2 effectively implying the correlation loss by component B during the interval of limit I.

Any interpretation of the frequency dependences must be compatible with the features of the molecular weight and temperature dependences, which reflect the same molecular dynamics with different phenomena. Below it will be shown that the combined analysis of all dependences forms a particularly critical test of theoretical predictions.

Theoretical Predictions for NMR Relaxation

Rouse chain dynamics[1] has been proposed under three different circumstances, namely, in polymer solutions, in melts with $M \ll M_c$, and—according to the Doi/Edwards model—in liquid polymer systems with any molecular weight in the time scale $\tau_s \ll t \ll \tau_e$ (limit I). This type of chain dynamics is characterized by the following frequency dependence of T_1:[30,31]

$$T_1 = -\frac{\beta}{\tau_s \ln(\omega\tau_s)} \quad (\omega\tau_s \ll 1; \beta = \text{const}) \tag{8}$$

T_1 dispersion data of solutions and melts with $M \ll M_c$ can indeed be described perfectly by this model (Figure 1a,c). Melts of "entangled" polymers in limit I, however, reveal a quite different behavior. Rouse dynamics entirely fails to explain the $\nu^{0.5}$ dispersion observed in this case (Figures 1b,d, 5, 8). An even more severe discrepancy of this model is the strong residual correlation obviously left over at the long-time end of limit I: Motions far beyond limit I are revealed by T_1 and T_2 relaxation spectroscopy although the rather isotropic segment reorientations caused by Rouse modes should prevent the visibility of such phenomena.

A further fact contradicting Rouse dynamics is that the influence of cross-linking (Figure 1d) is rather weak.[32] Merely with a mesh molecular weight less than about 3000 a somewhat different T_1 dispersion was found. In the length scales of limits I and II there must be restraints existing already without any cross-links.

de Gennes[4] predicted a proportionality $T_1 \propto \nu^{3/4}$ which should be valid in the time scale $\tau_e \ll t \ll \tau_R$ (limit II). This frequency dependence was never observed with melts or solutions of entangled polymers.

Thus a number of crucial predictions of tube theories fail to explain experimental findings. On the other hand, the fact that the Doi/Edwards limits of the mean-square segment displacement obviously have their analogues in the different regimes of the T_1 dispersion suggests that a similar model deviating only in a few basic points might provide better descriptions. The following concept aims at such a scheme.

Analysis of the Orientation Correlation Function into Components

Three components of the orientation correlation function can be distinguished:

Component A refers to the restricted rotational fluctuations within a Kuhn segment. A simplified but for our purposes sufficient approach of the corresponding orientation correlation function is

$$A(t) \approx a_1 e^{-t/\tau_s} + a_2 \tag{9}$$

The finite residual correlation of component A, $a_2 = 1 - a_1 > 0$, determines to what extent slower motions can contribute.

Component B is the orientation correlation function for reorientations mediated by translational displacements (RMTD). It is expected to be related to the segment dynamics according to limits I–III. Provided that the displacements of the segments are guided by the contour of the Kuhn chain or the primitive path, the following expression is valid:[33]

$$B(t) = \frac{1}{2D_1}\frac{d}{dt}\langle r_s^2(t)\rangle \tag{10}$$

D_1 is the segment diffusion coefficient along the curvilinear contour. It is independent of the molecular weight for times $t \ll \tau_R$.[3,29] r_s is the segment displacement in the center-of-mass frame of reference. This component therefore refers only to processes taking place in length scales within the polymer coils.

The longest time constant of the Doi/Edwards model, i.e., τ_d, defines a terminal decay of the orientation correlation function corresponding to the crossover to limit IV. In order to combine this final correlation loss with the diverse power laws expected to be valid in shorter time scales, we interpret it as a further component acting as a "cut-off" factor for component B.

Component C defined in this way is approximately given by the exponential function

$$C(t) \approx e^{-t/\tau_d} \tag{11}$$

This function depends strongly on the molecular weight as a consequence of the proportionality $\tau_d \propto M^3$. In the following section the influence of chain-end effects[29] as a competitive contribution important with chain lengths close to the critical value will be considered in addition.

The very different time scales of the three components guarantee their stochastic independence so that the total orientation correlation function can be written in the form

$$G(t) = A(t)\,B(t)\,C(t) \tag{12}$$

Component B Dominates. As a matter of fact, component C can be relevant for spin–lattice relaxation experiments only with molecular weights close to M_c. For higher molecular weights the fluctuation rates due to component C tend to be beyond the lower end of the relevant frequency window. In this case the approximation $C(t) \approx 1$ can be employed for T_1 and $T_{1\rho}$ (but not necessarily for T_2).

Component A, on the other hand, tends to be very fast so that in the time scale of the experiments $A(t) \approx a_2$ is often justified. Under such circumstances, that is, for $M \gg M_c$ and $\tau_s \ll t \ll \tau_d$, one has $G(t) \approx a_2 B(t)$.

With anomalous segment diffusion, i.e., $\langle r_s^2 \rangle = \alpha t^\kappa$ where $\kappa < 1$, the intensity function counterpart to the orientation correlation function $B(t)$ for contour guided segment displacements is

$$\mathcal{J}_B(\omega_i) \approx \frac{\alpha}{D_1}\kappa \sin\left(\frac{\pi(1-\kappa)}{2}\right)\Gamma(\kappa)\omega_i^{-\kappa} \qquad (13)$$

In the Doi/Edwards limits I–III the following cases can then be distinguished with respect to the frequency and molecular weight dependences of the spin–lattice relaxation times ($M \gg M_c$):

Limit I ($\tau_s \gg t \gg \tau_e$ or $\tau_e^{-1} \ll \omega_i \ll \tau_s^{-1}$):

$$T_1 \propto a_2 M^0 \omega_0^{1/2}; \quad T_{1\rho} \propto a_2 M^0 \omega_1^{1/2} \qquad (14)$$

Limit II ($\tau_e \ll t \ll \tau_R$ or $\tau_R^{-1} \ll \omega_i \ll \tau_e^{-1}$):

$$T_1 \propto a_2 M^0 \omega_0^{1/4}; \quad T_{1\rho} \propto a_2 M^0 \omega_1^{1/4} \qquad (15)$$

Limit III ($\tau_R \ll t \ll \tau_d$ or $\tau_d^{-1} \ll \omega_i \ll \tau_R^{-1}$):

$$T_1 \propto a_2 M^{-1/2} \omega_0^{1/2}; \quad T_{1\rho} \propto a_2 M^{-1/2} \omega_1^{1/2} \qquad (16)$$

Influence of Component A. At the high-frequency end of the accessible scale, the dynamics restricted to the length scale of the Kuhn segments (component A) dominates with the less flexible polymer species. One then expects $T_1 \propto a_1 M^0 \omega_0^0$. At extremely high frequencies, that is, $\omega_0 \gg \tau_s^{-1}$, the limit $T_1 \propto a_1 M^0 \omega_0^2$ follows from the simple correlation function suggested in eq 9.

Influence of the Terminal Decay (Component C). For molecular weights close to M_c at extremely low frequencies one expects

Limit IV ($t \gg \tau_d$ or $\omega_i \ll \tau_d^{-1}$):

$$T_1 \propto a_2 M^{-2} \omega_i^0; \quad T_{1\rho} \propto a_2 M^{-2} \omega_i^0 \qquad (17)$$

The behavior actually observed for $M \approx M_c$ is additionally influenced by chain-end effects to be discussed subsequently. The time scale of limit IV is, however, of major importance for the interpretation of transverse relaxation which is sensitive to considerably longer fluctuation times than spin–lattice relaxation.[15,24]

In limit IV the T_1 dispersion reaches a low-frequency plateau. This is the regime where the terminal decay by component C becomes relevant.

Characteristic exponents of the limiting power laws of the frequency dependences so far given are 0, $^1/_2$, and $^1/_4$ in coincidence with the experimental findings. Note that the only mean-square displacement limit leading to a molecular weight dependence of component B is limit III.

Chain-end Effects. Blocks consisting of N_e Kuhn segments at both chain ends do not "see" the topological constraints of the tube.[29] The limits II and III of component B are therefore expected to be irrelevant here. For the chain-end variant of component C we assume the correlation function $C_{ce} = \exp(-t/\tau_{ce})$. The influence of C_{ce} will be particularly strong for molecular weights close to M_c. The different dynamics of chain-end blocks was also found in a study of block copolymers of the type ABA[34] and was concluded from a recent computer simulation.[35]

The fraction of segments located in the chain-end blocks is $p = 2N_e/N \approx M_c/M$ ($M \geq M_c$). The weighting factor of the central segment block which is subject to "entangled behavior" is therefore $1 - p$. The correlation function for component C must be modified correspondingly. The molecular weight effective for tube disengagement is $M(1 - p)$. The effective tube disengagement time therefore is

$$\tau_{d,eff} = \frac{1}{\pi^2}\frac{N^3(1-p)^2}{N_e}\tau_s c^{3/2} \quad (M > M_c) \qquad (18)$$

The correlation function for component C of the chain-middle block is then assumed to be $C_{cm} = \exp(-t/\tau_{d,eff})$.

Total Correlation Functions for Spin–Lattice Relaxation. The dynamics in the central and in the chain-end segment blocks is expected to be different according to the scheme outlined above. In spite of this heterogeneity spin–lattice relaxation tends to be monoexponential because of the averaging effect of fast immaterial spin diffusion.[20] Strictly speaking the average should be formed with the correspondingly weighted relaxation rates. Formally it is however equivalent to form the average on the level of the correlation function. For spin–lattice relaxation, eq 12 thus can be replaced by

$$\begin{aligned} G_{sl}(t) &= pG_{ce}(t) + (1-p)G_{cm}(t) \\ &= pA(t)\,B_I C_{ce}(t) + (1-p)A(t)\,B_{I,II,III}(t)\,C_{cm}(t) \\ &\qquad \text{for } M > M_c \end{aligned} \qquad (19)$$

B_I and $B_{I,II,III}$ refer to the correlation functions of component B in the Doi/Edwards limits I–III. The chain-end correlation function $G_{ce}(t)$ solely refers to limit I.

Polymer chains with $M_w < M_c$ entirely consist of chain-end blocks, so to speak. In this case the weighting factor for the chain-end blocks is set $p = 1$. Apart from component A which is relevant in the short-time/high-frequency limit, the relaxation behavior should be governed by the Rouse mechanism, so that eq 8 is relevant. The correlation function of melts with $M < M_c$ in the long-time limit can tentatively and for simplicity also be equated with that of the the chain-end blocks, i.e.

$$G_{sl}(t) = A(t)\,B_I C_{ce}(t) \qquad \text{for } M < M_c \qquad (20)$$

Total Transverse Relaxation Functions. Averaging by immaterial spin diffusion is not effective for transverse relaxation so that the formal average formation on the level of correlation functions (eq 19) is no longer feasible.[15,29] Rather a superposition of the transverse magnetization signals of chain-end and chain-middle blocks has to be considered. That is

$$\begin{aligned} S(t) &= pS_{ce}(t) + (1-p)S_{cm}(t) \\ &= S(0)[p\exp\{-M_2\textstyle\int_0^t (t-\tau)G_{ce}(\tau)\,d\tau\} \\ &\quad + (1-p)\exp\{-M_2\textstyle\int_0^t (t-\tau)G_{cm}(\tau)\,d\tau\}] \end{aligned} \qquad (21)$$

$S_{ce}(t)$ and $S_{cm}(t)$ are the transverse magnetization signals of the chain-end and chain-middle blocks, respectively. These functions can be calculated by identifying the correlation functions $G_\omega(t)$ with the functions $G_{ce}(t)$ and $G_{cm}(t)$, respectively, as defined in eq 19.

Numerical Evaluation

For spin–lattice relaxation, the Fourier transform of the correlation functions eqs 19 or 20 was numerically evaluated decade by decade using the Gaussian quadrature method[36]

$$\mathcal{J}(\omega_i) = 2\int_0^\infty G(t)\cos(\omega_i t)\,dt \approx 2\int_l^u G(t)\cos(\omega_i t)\,dt \qquad (22)$$

The integration limits were chosen to be $l = 10^{-15}$ s and

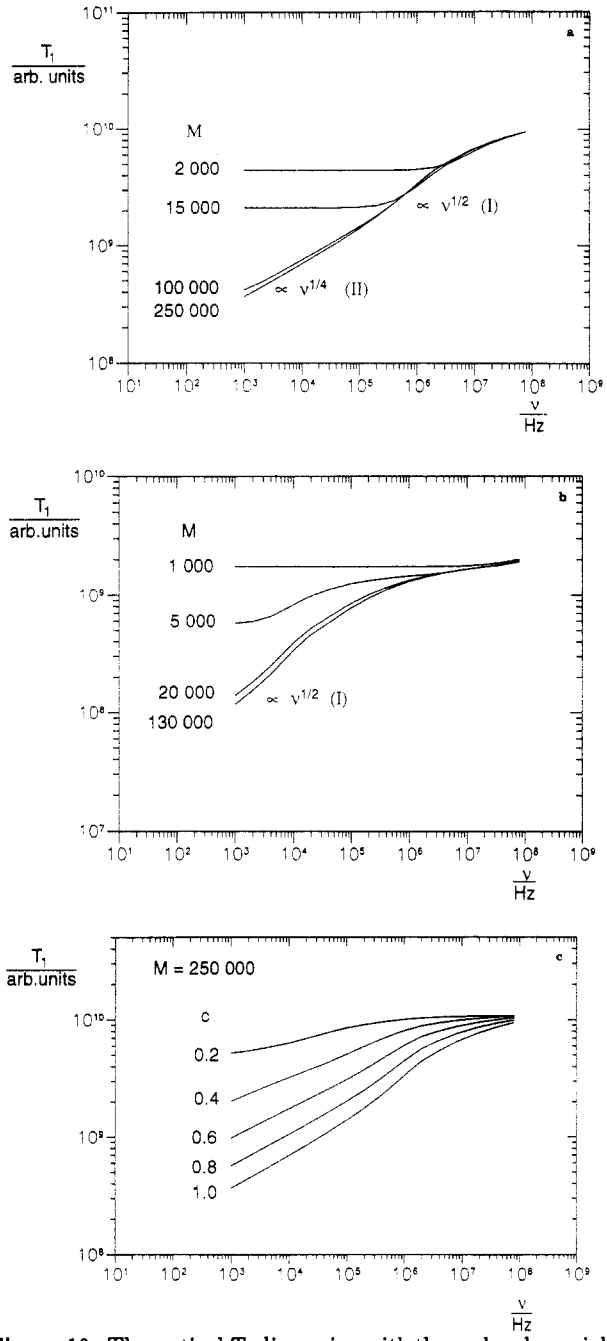

Figure 10. Theoretical T_1 dispersion with the molecular weight and the polymer concentration as curve parameters. The curves were evaluated on the basis of the correlation functions in eqs 19 and 20 and the formalism described in the text. Chain-end free-volume effects[38] which are relevant in reality for short chains were not taken into account. The parameters are as follows: (a) $a_1 = 0.96$; $\tau_s = 1 \times 10^{-10}$ s; $\tau_e = 2 \times 10^{-7}$ s; $\tau_{ce} = 1 \times 10^{-15} \times MM_c$ s ($M < M_c$); $\tau_{ce} = 1 \times 10^{-15} \times M_c^2$ s ($M > M_c$); $\tau_{d,eff} = (M/M_e)^3 (1 - p)^2\tau_e$ s; $M_c = 20\,000$; $M_e = 9000$. (The values were adapted to the PDMS melt data in Figure 1a.) (b) $a_1 = 0.98$; $\tau_s = 6 \times 10^{-10}$ s; $\tau_e = 3 \times 10^{-5}$ s; $\tau_{ce} = 2 \times 10^{-15} \times MM_c$ s ($M < M_c$); $\tau_{ce} = 2 \times 10^{-15} \times M_c^2$ s ($M > M_c$); $\tau_{d,eff} = (M/M_e)^3 (1 - p)^2\tau_e$ s; $M_c = 4000$; $M_e = 1400$. (The values were adapted to PE melt data.[15]) (c) Parameters as with Figure 10a modified by the polymer concentration (in percent by weight) as described in the text. For experimental data see Figure 1c.

$u = 10^{-1}$ s corresponding to the experimentally accessible frequency range. Above M_c the correlation function eq 19 was composed of the diverse limits of component B in such a way that a continuous function of time was formed. The crossover conditions are $B(t) = 1$ for $t \leq \tau_s$, $B_I(\tau_e) = B_{II}(\tau_e)$, and $B_{II}(\tau_R) = B_{III}(\tau_R)$.

Parts a and b of Figure 10 show the frequency dependences of the spin–lattice relaxation time calculated for polymer melts with different molecular weights below and above M_c. The parameters of the above formalism were chosen to adapt the theoretical curves to the experimental data for PDMS (see Figure 1a) and PE,[15] respectively, so that the frequency and molecular weight dependences are reproduced.

In Figure 10c, the influence of the polymer concentration on the frequency dependence of T_1 is shown. Apart from the concentration dependence of τ_d, the following relations were assumed to be valid for solutions:[37] $M_c(c) = M_c(c=1)/c$, $p(c) = M_c(c)/M$, and $a_2(c) = a_2(c=1)c^2$. For $c = 1$, i.e., melts, the parameters take the same values as in Figure 10a. The result corresponds to the experimental behavior shown in Figure 1c.

The crossover between limits II and III of component B, that is, from incoherent (molecular weight independent) to coherent (molecular weight dependent) segment motions, is of particular interest in context with transverse relaxation. In order to have smooth curves in the crossover region, component B was approximated for those two limits by

$$B_{II,III}(t) = e^x \operatorname{erfc}(\sqrt{x}) \qquad (23)$$

where $x = x(t) = (\xi_1 M^{-1} t + \xi_2 t^{3/2})^{1/2}$. ξ_1 and ξ_2 are numerical constants. Depending on whether the second or the first of the two terms of $x(t)$ dominates, we have the limits $M^0 t^{-3/4}$ and $M^{1/2} t^{-1/2}$ corresponding to $B_{II}(t)$ and $B_{III}(t)$, respectively. Note that the transition between the limits III and IV is already implied by the introduction of component C as a cutoff term of component B as outlined above. Note further that limit I normally refers to times too short to be relevant for the transverse relaxation behavior. This limit therefore was not considered explicitly in the calculations of the transverse relaxation decays. It was rather taken into account by an effectively reduced residual correlation a_2.

Figure 9 shows two representative transverse relaxation decays evaluated on the basis of eqs 21 and 23 for molecular weights below and above M_c. The curves are compared with experimental data[29] for PDMS melts. Above M_c the contributions of the chain-end blocks (slow decay) and the middle block (fast decay) can be distinguished.

Figure 11 shows the molecular weight dependence of T_2 (evaluated as the decay time to 1/e). The curves qualitatively mirror all features of the experimental data presented in a previous paper.[15] This refers in particular to the crossover phenomena observed at the characteristic molecular weights M_c and M_{BC}. (The experimental transverse relaxation decays were evaluated in the same way as those calculated numerically in this study.) The molecular weight dependence between M_c and M_{BC} refers to limits III and IV. The molecular weight independent plateau above M_{BC} reflects the dominance of limits I or II. T_1 at high frequencies and molecular weights is also independent of the molecular weight. This is a consequence of the dominating component A.[39]

Temperature dependences were treated assuming Arrhenius laws $\tau_i = \tau_{i\infty} \exp(E/k_B T)$ with the same apparent activation energy E for all time constants. Figure 12 shows the theoretical dependence T_2 on the reciprocal temperature. The essential features of experimental data[24] are reproduced again, in particular the crossover phenomena at the characteristic temperatures T_{AB} and T_S. These temperatures indicate the crossover between cases where the dynamics is governed by molecular weight dependent ($T \gg T_{AB}$) or molecular weight independent ($T_{AB} > T >$

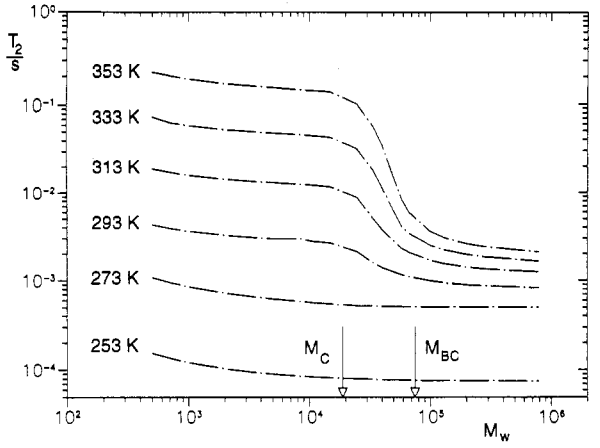

Figure 11. Theoretical molecular weight dependence of T_2 evaluated as the decay time to 1/e of the transverse relaxation function in eq 21 (see Figure 9). The two characteristic molecular weights, M_c and M_{BC}, indicate the crossover between cases where Rouse-like motions ($M \ll M_c$), M-dependent contour-guided motions ($M_c < M < M_{BC}$), and M-independent contour-guided motions are relevant. The M-dependent motions refer to limits III and IV, and the M-independent motions, to limits I and II, as described in the text. Chain-end free-volume effects[38] were not taken into account. The essential features of the experimental M_w dependences are reproduced.[15]

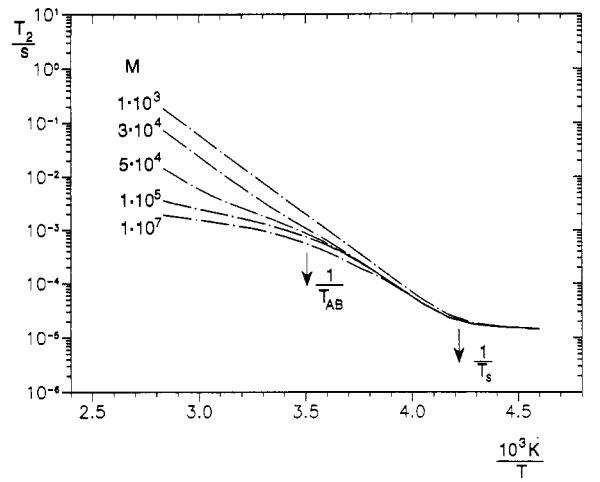

Figure 12. Theoretical temperature dependence of T_2 evaluated as the decay time to 1/e of the transverse relaxation function in eq 21 (see Figure 9). The two characteristic temperatures, T_{AB} and T_S, indicate the crossover between the limits of M-dependent ($T \gg T_{AB}$) or M-independent ($T_{AB} < T < T_S$) motions and of the limit where all chain modes are frozen in ($T \ll T_S$). The M-dependent motions refer to limits III and IV, and the M-independent motions, to limits I and II, as described in the text. Chain-end free-volume effects[38] were not taken into account. The features of the experimental temperature dependences are reproduced.[24]

T_S) motions and where all chain modes are frozen in ($T \ll T_S$). The molecular weight dependent motions refer to limits III and IV, the molecular weight independent motions, to limits I or II. The temperature dependences of T_1 and $T_{1\rho}$ are characterized by minima where $\omega\tau_s \approx 1$.[24,27]

Conclusions and Discussion

The main techniques employed in this study were field-cycling NMR relaxation spectroscopy and transverse NMR relaxation. The dynamic range of these methods is particularly wide and covers relatively low frequencies. There is a straightforward connection between the components of segment fluctuations and the relaxation quantities. A corresponding formalism has been outlined. NMR field-gradient studies of segment diffusion,[6-9] on the other hand, refer to a longer time scale. NMR relaxation thus covers the dynamic range between neutron spin-echo studies[10,11] at short times and NMR field-gradient experiments at long times.

For $M > M_c$, three peculiar power laws of the low-frequency dispersion of the spin–lattice relaxation times of polymer melts, namely, T_1, $T_{1\rho} \propto \nu^0$, $\nu^{0.25}$, and $\nu^{0.5}$ are evident. Seven different polymers were investigated so that the experimental findings can be considered to be of a universal nature.

The dynamic ranges in which these power laws appear coincide with the Doi/Edwards limits for the time dependence of the mean-square displacement so far as one can judge from the literature data available.

There is, however, a severe discrepancy with the Doi/Edwards theory: The Rouse dynamics expected in limit I could not be verified with melts above M_c. This model entirely fails to describe the relaxation data, while the T_1 dispersion of solutions and melts far below M_c can perfectly be rendered on this basis.

On the other hand, assuming that segment displacements are guided by the chain contour permits one to derive the experimental low-frequency T_1 dispersion directly from the limits of the time dependence of the mean-square segment displacement. The conclusion is that in limit I the segments tend to be displaced along the randomly coiled chain contour. The displacements in limit II take place along the primitive path which is the result of the topological constraints. That is, the peculiar exponent $^1/_4$ arises from a random walk (chain contour) on a random walk (primitive path). Limit III finally corresponds to the conventional reptation regime referring to coherent chain displacements along the primitive path. This interpretation is corroborated by the successful description of the molecular weight and temperature dependences of transverse relaxation on the same basis. In the light of this conclusion and our previous statistical thermodynamics study,[3] the Doi/Edwards tubelike region must be understood as the mean fluctuation range of lateral chain excursions ("folds") defining semi-independent subchains. A consequence of this is that the diffusion coefficient D_1 for displacements along the curvilinear path is independent of the chain length for $t \ll \tau_R$.

The failure of the $\nu^{3/4}$ law predicted by de Gennes[4] to describe the experimental T_1 dispersion in limit II appears now plausible: In its derivation no finite persistence of the segment orientation with displacements was permitted in contrast to the present concept. The persistence probability of the path thus plays a key role in the interpretation of the data.

The above discussion of NMR relaxation in polymers refers to the tube model in general. Further progress in our understanding of chain dynamics is expected from theories starting from first principles such as Schweizer's concept.[40,41] The appealing feature of this treatment is that a priori model assumptions such as the tube or Rouse dynamics are avoided throughout. An attempt to derive the spin–lattice relaxation dispersion directly on this basis has been undertaken and will be published elsewhere.[31]

Acknowledgment. We thank B. Striebel and J. Wiringer for excellent technical assistance and N. Fatkullin for helpful discussions. Financial support was received from the Deutsche Forschungsgemeinschaft (SFB 239).

References and Notes

(1) Doi, M.; Edwards, S. F. *The Theory of Polymer Dynamics*; Clarendon Press: Oxford, U.K., 1986.

(2) de Gennes, P.-G. *Scaling Concepts in Polymer Physics*; Cornell University Press: Ithaca, NY, 1979.
(3) Kimmich, R.; Köpf, M. *Progr. Colloid Polym. Sci.* **1989**, *80*, 8.
(4) de Gennes, P.-G. *J. Chem. Phys.* **1971**, *55*, 572.
(5) Lodge, T. P.; Rotstein, N. A.; Prager, S. *Adv. Chem. Phys.* **1990**, *79*, 1.
(6) Kimmich, R.; Unrath, W.; Schnur, G.; Rommel, E. *J. Magn. Reson.* **1991**, *91*, 136.
(7) Callaghan, P. T.; Coy, A. *Phys. Rev. Lett.* **1992**, *68*, 3176.
(8) Fleischer, G.; Fujara, F. *Macromolecules* **1992**, *25*, 4210.
(9) Rommel, E.; Kimmich, R.; Spülbeck, M.; Fatkullin, N., submitted for publication in *Prog. Colloid Polym. Sci.*
(10) Richter, D.; Fetters, L. J.; Huang, J. S.; Farago, B.; Ewen, B. *J. Non-Cryst. Solids* **1991**, *131–133*, 604.
(11) Richter, D.; Butera, R.; Fetters, L. J.; Huang, J. S.; Farago, B.; Ewen, B. *Macromolecules* **1992**, *25*, 6156.
(12) Noack, F. *Prog. NMR Spectrosc.* **1986**, *18*, 171.
(13) Kimmich, R. *Bull. Magn. Reson.* **1980**, *1*, 195.
(14) Kimmich, R. *Polymer* **1975**, *16*, 851.
(15) Kimmich, R.; Schnur, G.; Köpf, M. *Prog. NMR Spectrosc.* **1988**, *20*, 385.
(16) Weber, H.-W.; Kimmich, R.; Köpf, M.; Ramik, T.; Oeser, R. *Prog. Colloid Polym. Sci.* **1992**, *90*, 104.
(17) Huirua, T. M.; Wang, R.; Callaghan, P. T. *Macromolecules* **1990**, *23*, 1658.
(18) Callaghan, P. T. *Polymer* **1988**, *29*, 1951.
(19) Schneider, H.; Hiller, W. *J. Polym. Sci., Polym. Phys. Ed.* **1990**, *28*, 1001.
(20) Abragam, A. *The Principles of Nuclear Magnetism*; Clarendon Press: Oxford, U.K., 1961.
(21) Look, D. C.; Lowe, I. J. *J. Chem. Phys.* **1966**, *44*, 2995.
(22) Litvinov, V. M.; Lavrukhin, G. D.; Zhadnov, A. A. *Vysokomol. Soedin.* **1985**, *A27*, 2482.
(23) Burnett, L. J.; Rottler, C. L.; Laughon, D. H. *J. Polym. Sci., Polym. Phys. Ed.* **1978**, *16*, 341.
(24) Schnur, G.; Kimmich, R. *Chem. Phys. Lett.* **1988**, *144*, 333.
(25) Kremer, K.; Grest, G. S. *J. Chem. Phys.* **1990**, *92*, 5057.
(26) Grapengeter, H.-H.; Kosfeld, R.; Offergeld, H.-W. *Colloid Polym. Sci.* **1980**, *258*, 564.
(27) Ramik, T. Diploma thesis, University of Ulm, 1988.
(28) Fedotov, V. D.; Schneider, H. *Structure and Dynamics of Bulk Polymers by NMR-Methods, NMR 21*; Springer-Verlag: Berlin, 1989.
(29) Kimmich, R.; Köpf, M.; Callaghan, P. T. *J. Polym. Sci., Polym. Phys. Ed.* **1991**, *29*, 1025.
(30) Khazanovich, T. N. *Polym. Sci. USSR* **1963**, *4*, 727.
(31) Fatkullin, N.; Kimmich, R.; Weber, H. W. *Phys. Rev. E*, in press.
(32) Andrady, A. L.; Llorente, M. A.; Mark, J. E. *Polym. Bull.* **1991**, *26*, 357.
(33) Kimmich, R.; Weber, H.-W. *J. Chem. Phys.*, in press.
(34) Köpf, M.; Schnur, G.; Kimmich, R. *Macromolecules* **1988**, *21*, 3340.
(35) O'Connor, N. P. T.; Ball, R. C. *Macromolecules* **1992**, *25*, 5677.
(36) Abramowitz, M., Stegun, I. A., Eds. *Handbook of Mathematical Functions*; Applied Mathematics Series 55; National Bureau of Standards: Washington, D.C., 1970.
(37) Köpf, M.; Schnur, G.; Kimmich, R. *J. Polym. Sci.: Polym. Lett.* **1988**, *26*, 319.
(38) Ferry, I. D. *Viscoelastic Properties of Polymers*; Wiley: New York, 1980.
(39) Kimmich, R.; Rosskopf, E.; Schnur, G.; Spohn, K.-H. *Macromolecules* **1985**, *18*, 810.
(40) Schweizer, K. S. *J. Chem. Phys.* **1989**, *91*, 5802.
(41) Schweizer, K. S. *J. Chem. Phys.* **1989**, *91*, 5822.